Sustainable Energy & Fuels

ROYAL SOCIETY OF CHEMISTRY

PAPER

View Article Online
View Journal | View Issue

Cite this: *Sustainable Energy Fuels*, 2026, **10**, 2478

Boosted hydrogen production *via* binder-assisted immobilization of hydrogen boride sheets on cathodes

Masaki Imura,[a] Yuta Yamamoto,[a] Yohei Cho,[a] Akira Yamaguchi,[a] Shin-ichi Ito,[b] Yasuyuki Hikita,[c] Takahiro Kondo *[bde] and Masahiro Miyauchi *[ae]

Hydrogen boride (HB) sheets are attractive solid-state hydrogen carriers because of their safe, lightweight, and light-induced dehydrogenation properties. Previously, electrolytic hydrogen release under cathodic bias was reported for dispersed HB sheets. In this paper, we demonstrate that the immobilization of HB sheets on an electrode enhances their dehydrogenation rates by facilitating direct electron injection from the electrode into the HB sheets. HB sheets were immobilized on a carbon paper electrode using coating solutions containing HB sheets, various polymeric binders, and a solvent. Among various binders, aramid demonstrated excellent adhesion of HB sheets to an electrode and a high hydrogen release rate under cathodic bias. To further enhance the dehydrogenation rate, we have additionally introduced electroconductive graphene into the coating solutions to fix the film of HB sheets/aramid/graphene composites onto carbon electrodes. The optimum weight ratio of HB/aramid/graphene was 1/2/1, yielding a high dehydrogenation rate under cathodic bias. Electrochemical impedance spectroscopy analysis revealed a significant decrease in charge transfer resistance upon the addition of graphene. The present immobilized film provides a superior system compared with the conventional dispersed one for hydrogen release.

Received 6th February 2026
Accepted 16th April 2026

DOI: 10.1039/d6se00145a

rsc.li/sustainable-energy

1. Introduction

The global demand for hydrogen has steadily increased due to its role as a clean alternative fuel. Thus, the development of hydrogen carriers is essential for overcoming key challenges in hydrogen storage, transportation, and distribution. Hydrogen in its gaseous form has a low volumetric energy density and requires storage under high pressure or at cryogenic temperatures, posing challenges related to safety, cost, and infrastructure.[1] Advanced hydrogen carriers such as liquid organic hydrogen carriers (LOHCs),[1–3] metal hydrides,[1,4] and ammonia[1,2,7] offer safer, more efficient, and scalable alternatives for storing and transporting hydrogen. Furthermore, solid-state hydrogen carriers have been studied;[5,6] however, their hydrogen capacities are limited to date.

Computational studies have predicted the stability of planar boron hydride and its potential application as a hydrogen storage material.[8] It is also predicted to have several polymorphs[8] as well as unique mechanical and electronic properties.[9–11] In 2017, hydrogenated borophene was synthesized *via* a proton exchange process from magnesium diboride, which has two-dimensional boron layers and magnesium ions between them.[12] Hydrogenated borophene is also called "hydrogen boride (HB) sheets" rather than boron hydride due to the presence of negatively charged boron and protons. HB sheets have a high gravimetric hydrogen capacity (8.5 wt%). Several kinds of intriguing properties of HB sheets have been empirically found, such as solid acidity,[13,14] reductive capability and support for catalysts,[15–21] hydrogen production with external stimuli,[12,21–26] and thermal- and photostability after modification with pyrazine.[27]

In addition, electrolytic hydrogen production from HB sheets under low cathodic bias has recently been reported.[26] Most of the hydrogen in the HB sheets was released over 48 hours. However, HB sheets were dispersed in acetonitrile, resulting in poor physical contact between HB sheets and the electrode. Overcoming this hurdle presents an opportunity to improve the reaction system and achieve higher dehydrogenation rates.

In battery technology, binders are commercially used to immobilize a mixture of electrochemically active materials and a conductive additive (*e.g.*, graphene) on a current collector.[28]

[a]*Department of Materials Science and Engineering, School of Materials and Chemical Technology, Institute of Science Tokyo, Meguro-ku, Tokyo 152-8552, Japan. E-mail: miyauchi@mct.isct.ac.jp*

[b]*Department of Materials Science, Institute of Pure and Applied Sciences, University of Tsukuba, 1-1-1 Tennodai, Tsukuba, Ibaraki 305-8573, Japan*

[c]*Advanced Research and Innovation Center, DENSO CORPORATION, Nisshin, Aichi 470-0111, Japan*

[d]*The Advanced Institute for Materials Research, Tohoku University, 2-1-1 Katahira, Aoba-ku, Sendai, Miyagi 980-8577, Japan*

[e]*Hydrogen Boride Research Center, Tsukuba Institute for Advanced Research (TIAR), University of Tsukuba, 1-1-1 Tennodai, Tsukuba, Ibaraki 305-8573, Japan*

While polymeric binders are regarded as insulators, the inclusion of conductive additives ensures that the electrodes maintain good electrical conductivity.[29,30] A variety of binders have been commonly used. For example, poly(tetrafluoroethylene) (PTFE) is a conventional binder for aqueous solution. Nafion, a sulfonated form of PTFE, is commonly used in supercapacitors.[29,30] Poly(vinylidene difluoride) (PVDF) is the most widely used binder in lithium-ion batteries due to its excellent chemical and electrochemical stability along with robust mechanical properties.[29,30] It is also known that polymers with carboxyl groups such as carboxymethyl cellulose (CMC) and poly(acrylic acid) (PAA) allow for strong interactions with materials, resulting in good adhesion properties.[29,30] Aramid materials are sometimes used as binders due to their tensile strength, thermal stability, and durability.[31–34] Recent work has demonstrated that branched aramid nanofibers (BANFs), nanoscale Kevlar-derived fibers, can serve as effective binders for mechanically robust lithium-ion battery electrodes.[33] In this approach, BANFs are combined with lithium iron phosphate cathode particles or silicon anode particles together with reduced graphene oxide (rGO). The strong hydrogen-bonding interactions between BANFs and rGO facilitate efficient load transfer throughout the composite, resulting in electrodes with significantly enhanced mechanical integrity.

In this study, we report on the screening of binders to immobilize HB sheets onto carbon paper electrodes and improve hydrogen release rates from them. We found aramid to be an effective binder to immobilize HB sheets. The hydrogen release rate from the HB/aramid composite film under cathodic bias was higher than that from the dispersed HB system, even though polymeric binders like aramid are generally known to be insulators. Further, we successfully promoted the hydrogen release rate by adding graphene as a conductive additive. An HB/aramid/graphene weight ratio of 1/2/1 provided the best balance between adhesion and hydrogen-production performance.

2. Experimental

2.1. Synthesis of HB sheets

HB sheets were synthesized *via* a cation exchange process from magnesium diboride (MgB_2) using proton exchange resin in accordance with previous reports.[12,26] 0.5 g of MgB_2 (99%; Sigma-Aldrich, St. Louis, MO, US) and 30 mL of proton exchange resin (Amberlite IR120B, H^+ form; Organo Corporation, Kyoto, Japan) were added to 200 mL of acetonitrile (99.5%; FUJIFILM Wako Chemical Industries Co., Ltd, Osaka, Japan) under a nitrogen atmosphere, and they were stirred at 450 rpm for 2 days at room temperature. The products were then cooled to 233 K and filtered (Omnipore 0.2 μm, Merck Millipore Ltd, Billerica, MA) three times to remove byproducts. We additionally conducted a water treatment of the HB sheets, which stabilizes them.[35,36] 0.223 g of HB sheets were soaked in 10 mL of ultrapure water for a day. They were then dried at 85 °C under vacuum to obtain stabilized HB sheets. Subsequently, 30 mL of acetonitrile was added to the product. They were then cooled to 233 K for an hour under a nitrogen atmosphere and filtered to remove boric acid.

2.2. Preparation of binders

Aramid was provided by TEIJIN LIMITED. A 5% Nafion™ Dispersion Solution DE520 CS type was purchased from FUJIFILM Wako Pure Chemical Corporation. The other binders, poly(vinylidene difluoride) (PVDF), carboxymethyl cellulose (CMC), poly(tetrafluoroethylene) (PTFE), polyurethane (PU), styrene-butadiene rubber (SBR), and poly(acrylic acid) (PAA), were included in a binder kit (7 × 25 mL) from Redox.me. 5 g of binder was added to *N*-methyl-2-pyrrolidone (NMP) (99%; FUJIFILM Wako Chemical Industries Co., Ltd, Osaka, Japan) to a final volume of 100 mL.

2.3. Preparation of HB-immobilized electrodes

Carbon paper (TGP-H-60, Toray Industries Inc., Osaka, Japan) was cut into 1 × 1.5 cm^2 pieces. It was soaked in aqueous ethanol under ultrasonication for 5 min and additionally soaked in ultrapure water under the same conditions and duration. It was then dried at 40 °C for 30 min. Meanwhile, HB sheets (and graphene as necessary) were added to NMP and mixed with a vortex mixer. A binder dissolved in NMP was added to the mixture of HB sheets (and graphene) and NMP, and the solution was mixed again. The slurry was drop-cast onto a 1 × 1 cm^2 area of the carbon paper and dried in a vacuum oven at 80 °C for 2 hours. In this paper, the electrodes with HB sheets and binders are hereafter referred to as HB-immobilized electrodes and are denoted as "HB + binder electrode", where the term "binder" is substituted for the name of the binder used. In addition, the HB + aramid electrode with graphene is denoted as the "HB + aramid + graphene electrode". For preparing electrodes without binders, referred to as (None), HB sheets dispersed in NMP were drop-cast onto the electrodes and dried in the same manner. We also prepared electrodes coated with aramid and graphene, denoted as "aramid + graphene electrode". In addition, electrolysis of dispersed HB sheets in acetonitrile was conducted using bare carbon paper, and we compared its hydrogen release rate with that from immobilized HB sheets by various binders on carbon paper electrodes.

2.4. Characterization

Transmission electron microscope (TEM) images were taken using a JEOL-2010F (JEOL Ltd, Tokyo, Japan). Fourier-transform infrared (FT-IR) spectra were recorded using an FT/IR-6100 (JASCO Co., Ltd, Tokyo, Japan) with an attenuated total reflection (ATR) unit (MIRacle 025-18xx). X-ray photoelectron spectroscopy (XPS) was performed using a JPS 9010 TR instrument (JEOL Ltd, Tokyo, Japan) with a Mg-K_α X-ray source. The binding energies were calibrated using the peak of the C 1s orbital. Scanning electron microscopy (SEM) was performed using a JCM-7000 NeoScope™ (JEOL Ltd, Tokyo, Japan).

2.5. Mass loss of HB sheets from HB-immobilized electrodes

3 mg of stabilized HB sheets and 0.75 mg of binder were used for preparing HB-immobilized electrodes. These electrodes were immersed in 20 mL of acetonitrile for 5 min. Subsequently, the weight of the electrodes was measured to determine the

mass loss of the HB sheets/binder composite. We also prepared electrodes without HB sheets by using 0.75 mg of binders. These electrodes were also immersed in acetonitrile in the same manner with the mass-loss evaluation of HB-immobilized electrodes. The net HB sheets loss was calculated by subtracting the mass loss of HB sheets and that of the binder-only electrode conditions.

2.6. Electrochemical measurements

The electrochemical measurements were performed using a potentiostat (HZ-7000; HOKUTO DENKO Co., Ltd, Japan) and a single compartment closed cell. HB-immobilized electrodes or bare carbon paper were used as working electrodes. A platinum spiral electrode and an Ag/Ag^+ electrode were used as the counter and the reference electrodes, respectively. Tetrabutylammonium hexafluorophosphate ($TBAPF_6$, 97.0%, FUJIFILM Wako Pure Chemical Industries Ltd, Osaka, Japan) was used as an electrolyte. 0.79 g of $TBAPF_6$ was added to 20 mL of acetonitrile to prepare 0.1 M of $TBAPF_6$/acetonitrile solution for electrolysis. For the evaluation of hydrogen release properties, electrochemical cathodic bias was applied at a constant potential of −1 V *vs.* Ag/Ag^+ for 30 min. The hydrogen concentration was measured using a gas chromatograph equipped with a thermal conductivity detector (GC-2014AT; Shimadzu Co., Ltd, Japan). Electrochemical impedance spectroscopy (EIS) was conducted at open circuit potential with an amplitude of 10 mV and a frequency ranging from 10 kHz to 100 mHz.

3. Results and discussion

3.1. Characterization of pristine and immobilized HB sheets

Fig. 1a shows a transmission electron microscopy (TEM) image of pristine HB sheets, displaying a thin and sheet-like structure. As shown in Fig. 1b, the Fourier transform infrared (FT-IR) spectrum of pristine HB sheets exhibits B–H and B–H–B bonds: B–H stretching corresponds to ~2500 cm^{-1}, B–H bending to ~700 and ~1000 cm^{-1}, and B–H–B stretching to ~1350 cm^{-1} respectively.[37] In Fig. 1c, the X-ray photoelectron spectroscopy (XPS) spectrum of pristine HB sheets exhibits two types of boron species: one corresponds to boron species ($B^{\delta-}$) originating from the HB sheets themselves, while the other minor peak is attributed to positive boron species ($B^{\delta+}$) owing to contamination from oxidized boron species as a byproduct. Similar to several previous studies,[12,37] the signal of the $B^{\delta+}$ species was limited, indicating the successful synthesis of HB sheets in the present study. In Fig. 1d, FT-IR spectra of pristine HB sheets and the HB sheets/aramid composite with a weight ratio of 1/2 reveal a slight shift of the peak originating from the B–H bond, indicating the interaction between HB sheets and aramid. Fig. 1e demonstrates the XPS spectrum of the HB sheets with aramid, the optimal binder as mentioned later, with a weight ratio of HB/aramid = 1/2. Although a strong $B^{\delta-}$ peak and a weak $B^{\delta+}$ peak were observed, similar to the pristine HB sheets' case, the additional peak appeared between them around 191 eV. There are no candidates other than boron, indicating that this additional peak would originate in boron species, which interact with aramid. Indeed, XPS spectra of hexagonal boron nitride and its hydroxylated form show binding energies of 190.6 and 190.9 eV attributed to B–N and B–O bonds, respectively,[38] corresponding to the unknown peak in Fig. 1e. Therefore, the additional peak is attributed to boron species in HB sheets, which interact with functional groups of aramid. Other studies reported that boron of HB sheets interacts with nitrogen from phenanthroline[23] and amide groups from bovine serum albumin,[39] which is widely used as a protein concentration standard. Fig. 1f shows the surface morphology

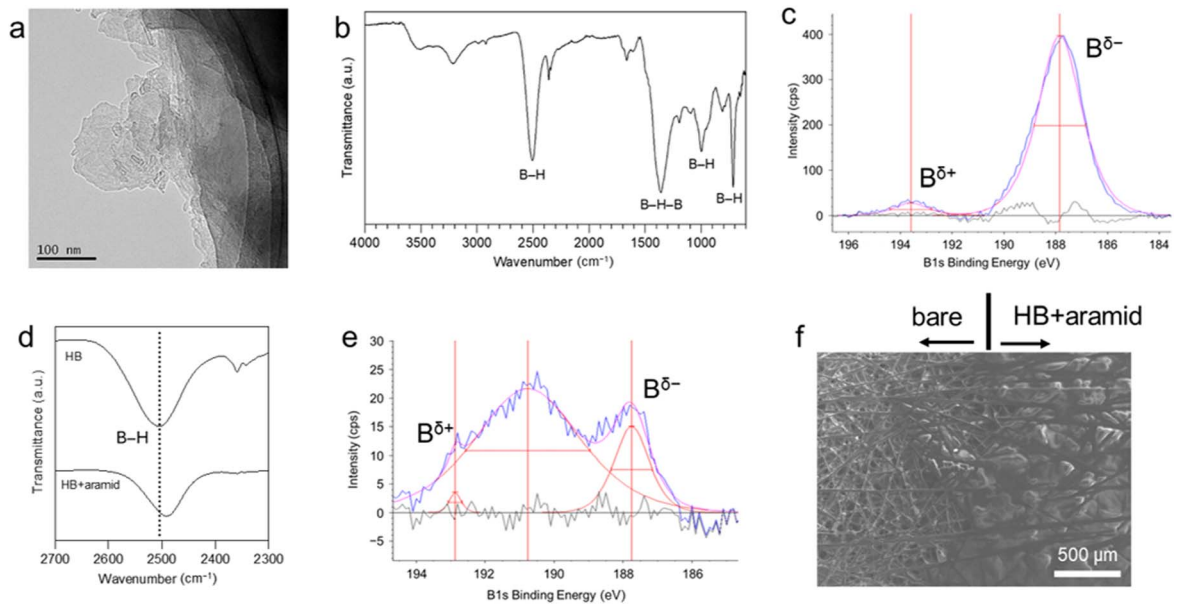

Fig. 1 (a)TEM image, (b) FT-IR spectrum, and (c) XPS spectrum of HB sheets. (d) FT–IR spectra of HB sheets and the HB/aramid composite and (e) XPS spectrum of the HB/aramid composite. (f) SEM image of carbon paper showing the bare part and modified part with HB sheets and aramid. Panels c and e show measured spectra in blue, Gaussian peak fits in red and residuals in black.

at the edge part of the HB + aramid film on the carbon paper electrode. In this figure, the uncoated region is visible on the left side, while the HB + aramid film was coated on the right side. Bare carbon paper displays numerous carbon fibers, whereas they are invisible on carbon paper with HB + aramid. Electron probe microanalyzer (EPMA) analysis also revealed the existence of HB sheets on the carbon paper electrode (Fig. S1 in the SI). These results suggest that the mixture of HB sheets and aramid is successfully coated on carbon paper. Additionally, FT-IR spectra of HB sheets and those with each binder are shown in Fig. S2 in the SI. Signals of the B–H bond were seen in all electrodes, indicating the immobilization of HB sheets on electrodes by binders.

3.2. Screening of binders

3.2.1. Mass loss of HB sheets from HB-immobilized electrodes. Before the evaluation of electrolytic hydrogen release properties, we investigated the adhesion stability of immobilized HB sheet electrodes by immersing them in acetonitrile for 5 min. Their masses were measured to assess the extent of HB sheet detachment during immersion. Since both HB sheets and binders could potentially peel off, we measured the mass change of electrodes containing only binders under the same conditions. The latter values were then subtracted from the former to calculate the net mass loss of the HB sheets. As shown in Table 1, aramid immobilized HB sheets onto a carbon electrode most effectively. These results indicate the affinity between HB sheets and amide groups of aramid, resulting in good adhesion. On the other hand, compared with aramid, binders with a carboxylic group, such as CMC and PAA, were less effective. CMC and PAA polymers are normally regarded as good binders, as mentioned in the Introduction. A previous study reported that HB sheets have limited interaction with carboxylic groups of dye molecules, which are often utilized for dye-sensitized solar cells.[24] The present result indicates that organic molecules with carboxyl groups do not adhere well to HB sheets.

Table 1 Mass loss of HB + binder electrodes, binder-only electrodes and net HB sheets[a]

Binder	HB + binder loss/mg	Binder loss/mg	Net HB loss/mg
(None)	3.0	0.0	3.0
Nafion	3.4	0.5	2.9
PVDF	3.1	0.1	3.0
PTFE	2.2	0.1	2.1
SBR	2.6	0.1	2.5
CMC	2.8	0.2	2.6
PAA	2.3	0.1	2.2
PU	2.5	0.1	2.4
Aramid	1.6	0.0	1.6

[a] Note: the mass loss of the HB + binder electrode was evaluated after soaking the electrode in acetonitrile for 5 min. The mass loss of the binder-only electrode was measured by soaking the binder adhered to the carbon paper under the same conditions. The net HB loss was calculated by subtracting the binder loss from the HB + binder loss.

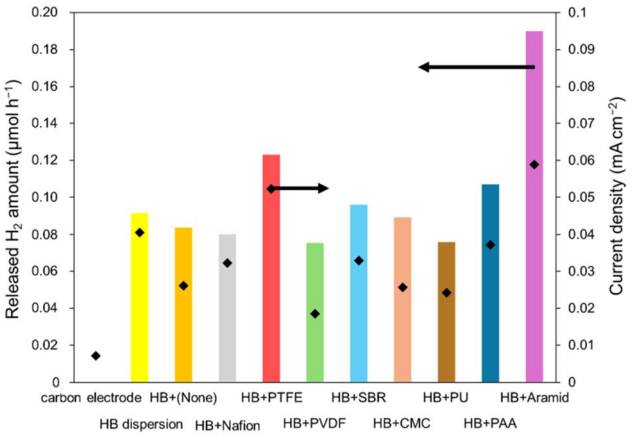

Fig. 2 Hydrogen production from HB-immobilized electrodes with several sorts of binders. Black diamonds represent current densities, while bars show released H_2.

3.2.2. Hydrogen production properties. We evaluated the electrolytic hydrogen release properties of HB-immobilized electrodes. As a control experiment, we additionally conducted electrolysis of dispersed HB sheets in which a bare carbon paper electrode was used as a working electrode. Fig. 2 shows the results of hydrogen production under cathodic bias. The hydrogen production amount from the HB + aramid electrode for 1 h corresponded to 0.4% of the theoretical maximum amount from HB sheets, which was significantly larger than those obtained with the other binders. While current densities in the experiments using the HB + aramid electrode and HB + PTFE electrode are nearly the same, the amount of hydrogen released differs significantly, indicating the effective immobilization of HB sheets by aramid. In some cases, the hydrogen production ability was lower than that in the dispersion system due to the insulating nature of polymeric binders and lower current density. Considering these results, the HB + aramid electrode is the best candidate for hydrogen production under electrolytic stimulation.

Next, we evaluated the aramid amount dependence on the hydrogen production performance. As illustrated in Fig. 3, a volcano-shaped trend in hydrogen production was observed, suggesting a trade-off between the adhesion and insulating nature of aramid. At lower ratios of aramid to HB, the aramid adhered less to HB sheets without suppressing conductivity. In contrast, a higher aramid/HB ratio exhibited superior adhesion but inferior conductivity. The optimum aramid/HB weight ratio was 0.25 for the high hydrogen release rate. Furthermore, the net mass loss of HB sheets that were peeled from the HB + aramid electrodes is documented in Table S1. It shows that the mass loss is prevented by the addition of the aramid binder. In this table, mass loss data after electrolysis are also shown, and the hydrogen production had little effect on the detachment of HB sheets and aramid.

3.2.3. Effect of aramid on charge transfer resistance. We conducted the EIS measurements for electrochemical cells using the HB + aramid electrode and the bare carbon paper with dispersed HB sheets, respectively. The composition of HB/

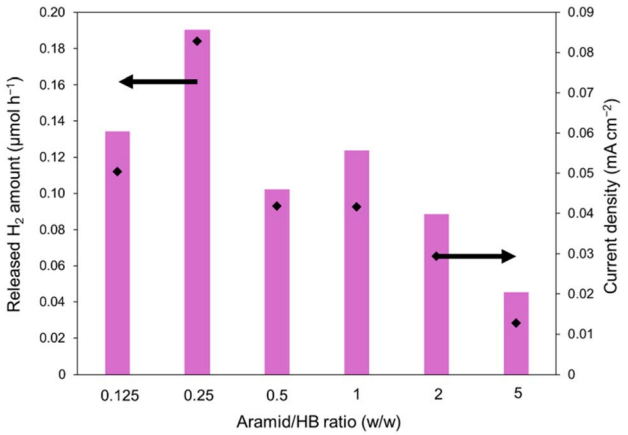

Fig. 3 Hydrogen production from HB + aramid electrodes with several amounts of aramid.

aramid in the composite electrode was fixed at 1/2. Fig. 4 shows the smaller semicircle diameter (*i.e.*, charge transfer resistance, R_{ct}) in the HB + aramid system compared to that of the dispersed HB system. This reduction in R_{ct} is attributed to improved physical contact between HB sheets and the carbon paper electrode, which enhances interfacial electron transfer. However, the R_{ct} of the HB + aramid system remains relatively high, likely due to the insulating nature of aramid. The incorporation of conductive materials such as graphene into the HB + aramid composite is anticipated to overcome the insulating nature of binders. The effect of the addition of graphene is discussed in the next section.

3.3. Effect of graphene as a conductive additive

We prepared HB + aramid + graphene electrodes, where graphene was used as a conductive additive. Fig. 5 shows a relationship between the HB/aramid/graphene ratio and hydrogen production ability. Significant hydrogen production was observed when we chose the electrode with a HB/aramid/

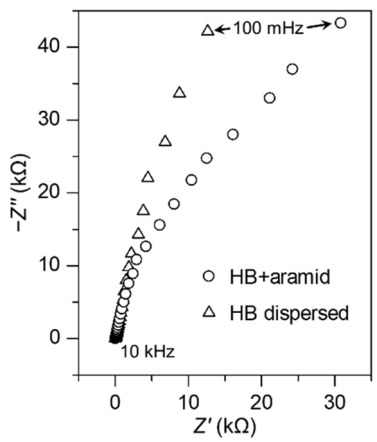

Fig. 4 Nyquist plot of the system using the HB + aramid electrode (circles) and a bare carbon paper electrode along with dispersed HB sheets (triangles).

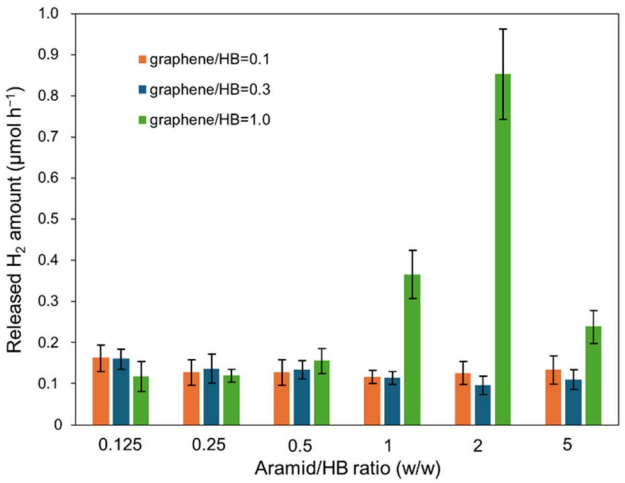

Fig. 5 Hydrogen production from HB + aramid + graphene electrodes with several amounts of aramid and graphene. Bars represent the mean values, with error bars indicating the standard deviation ($n = 3$).

graphene weight ratio of 1/2/1. In this case, the amount of hydrogen released from HB sheets for 1 h corresponded to 2% of the maximum obtainable amount, which was comparable to the previous report under different experimental conditions.[26] In the case of graphene/HB = 0.1 and 0.3, hydrogen production abilities were not higher than those without graphene. This is likely because the low concentration of graphene was insufficient to form a conductive network and block active sites on the electrode. Another probable reason is that aramid and graphene interacted *via* π–π stacking,[34,40] causing the HB sheets to be immobilized between the graphene sheets and become inert due to the large interlayer spacing. The excess aramid likely increased the interlayer spacing. A previous study regarding supercapacitors with rGO/aramid nanofiber (ANF) composite electrodes shows a decrease in capacitance with increasing ANF content because rGO was diluted, and the sheet-to-sheet contact between rGO layers was reduced.[34] Even in the case of graphene/HB = 1.0 with aramid/HB = 0.125, 0.25 and 0.5, hydrogen production ability was lower than that without graphene, probably because poor adhesion properties caused graphene detachment, thereby reducing the graphene content. For aramid/HB ≥ 1.0 and graphene/HB = 1.0, it shows higher hydrogen production ability than that without graphene, indicating both sufficient graphene content and good adhesion. Fig. S3 shows FT–IR spectra of HB + aramid + graphene electrodes before and after the reaction.

As shown in Fig. 6, EIS measurements were performed to evaluate the effect of graphene incorporation. While the solution resistance (R_s) was nearly identical across all systems, R_{ct} showed significant differences. Compared to the results in Fig. 4, a substantial reduction of R_{ct} was observed upon the addition of graphene. Furthermore, the HB + aramid + graphene electrode exhibited an R_{ct} approximately one order of magnitude lower than that of the aramid + graphene electrode with dispersed HB sheets. As shown in Table S3 in the SI, the R_{ct} of the HB + aramid + graphene system was 65.8 Ω, whereas that

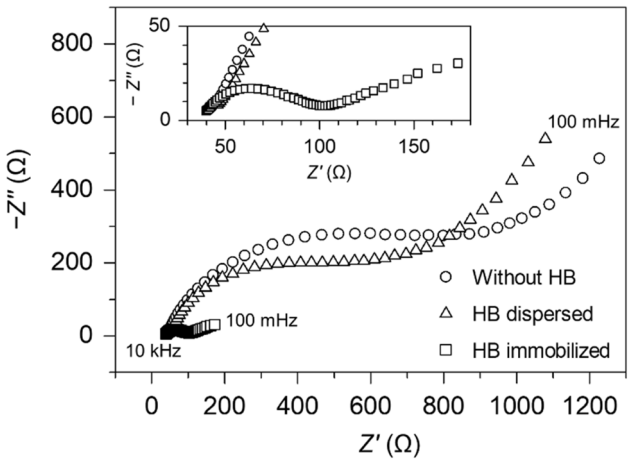

Fig. 6 Nyquist plots of the system without HB sheets (circles), that of the aramid + graphene electrode with dispersed HB sheets (triangles), and that of the HB + aramid + graphene electrode (squares), respectively. The measurements were conducted at open circuit potential. The inset shows the same plots with different scales.

of the aramid + graphene system with dispersed HB sheets was 520 Ω. Fig. S4 in the SI shows the equivalent circuit used for the fitting, and Table S3 summarizes the fitted parameters, including R_s, R_{ct}, and the other relevant parameters. In the case of the HB + aramid + graphene electrode, the Nyquist plot in the low frequency region shows a linear trend with a slope smaller than 45°, suggesting finite diffusion behavior. These results indicate that the incorporation of graphene improves charge transfer within the composite and enhances the electrochemical performance of immobilized HB sheets.

3.4. Hydrogen production from immobilized HB sheets and other proton sources

We finally compared hydrogen production from the HB + aramid + graphene electrode at a HB/aramid/graphene ratio of 1/2/1 with that from other proton sources: ultrapure water, formic acid, and HB sheets (without immobilization), all in identical molar amounts, were added to acetonitrile, respectively. In addition, we conducted a control experiment without any proton sources (blank). As shown in Fig. 7, the HB + aramid + graphene electrode produced the largest amount of hydrogen among the proton sources used. These results reveal that the immobilization of HB sheets improved the hydrogen release performance and HB sheets can release their hydrogen more efficiently than the other proton sources such as water and formic acid.

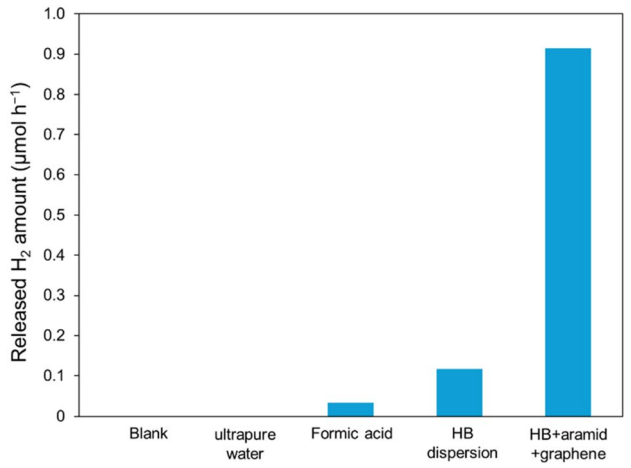

Fig. 7 Hydrogen production from the HB + aramid + graphene electrode and from various proton sources *via* electrolysis using the aramid + graphene electrode.

4. Conclusions

In this study, we successfully prepared HB-immobilized electrodes with binders. Among the binders tested, aramid proved most effective for immobilizing HB sheets onto an electrode for electrolytic hydrogen release, owing to the strong interaction between HB sheets and amide groups of aramid. We optimized the aramid/HB ratio to achieve a balance between strong adhesion and high hydrogen release rates. For more efficient hydrogen release, conductive graphene was added to the HB + aramid composite. We found that the electrode with an HB/aramid/graphene ratio of 1/2/1 exhibited the highest hydrogen release performance among various compositions. Furthermore, we conducted EIS and found that graphene caused a significant decrease in charge transfer resistance. Finally, we compared the hydrogen production ability from electrodes with HB/aramid/graphene = 1/2/1 with those from the other proton sources like water and formic acid. The HB + aramid + graphene electrode exhibited the most efficient dehydrogenation compared with the dispersed system and/or to the other proton sources.

Author contributions

M. I.: data curation (equal), formal analysis (lead), investigation (equal), methodology (supporting), validation (equal), visualization (lead), writing – original draft (lead), and writing – review & editing (equal). Y. Y.: conceptualization (supporting), data curation (equal), formal analysis (supporting), investigation (equal), methodology (equal), validation (equal), and visualization (supporting). Y. C.: project administration (supporting), supervision (supporting), and writing – review & editing (equal). A. Y.: project administration (supporting), resources (supporting), supervision (supporting), and writing – review & editing (equal). S–I. I.: formal analysis (supporting), methodology (supporting), investigation (supporting), and resources (supporting). Y. H.: supervision (supporting) and writing – review & editing (supporting). T. K.: conceptualization (lead), funding acquisition (lead), investigation (supporting), methodology (supporting), resources (supporting) and writing – review & editing (lead), and M. M.: conceptualization (lead), funding acquisition (lead), methodology (equal), project administration (lead), resources (lead), supervision (lead), writing – original draft (equal), and writing – review & editing (lead)

Conflicts of interest

There are no conflicts to declare.

Data availability

The data supporting this article have been included as part of the supplementary information (SI). Supplementary information is available. See DOI: https://doi.org/10.1039/d6se00145a.

Acknowledgements

The aramid binder was supplied from TEIJIN LIMITED. The TEM image was obtained at the Open Facility Centre of the Institute of Science Tokyo. We gratefully acknowledge financial support from JSPS KAKENHI (23K17953, 23K26735, 23K26536, 24H02204, and 25K22213). This study was partially supported by DENSO CORPORATION.

References

1 L. Schlapbach and A. Züttel, Hydrogen-storage materials for mobile applications, *Nature*, 2001, **414**(6861), 353–358.
2 A. Lin and G. Bagnato, Revolutionising energy storage: the Latest Breakthrough in liquid organic hydrogen carriers., *Int. J. Hydrogen Energy*, 2024, **63**, 315–329.
3 P. M. Modisha, C. N. M. Ouma, R. Garidzirai, P. Wasserscheid and D. Bessarabov, The Prospect of Hydrogen Storage Using Liquid Organic Hydrogen Carriers, *Energy Fuels*, 2019, **33**(4), 2778–2796, DOI: 10.1021/acs.energyfuels.9b00296.
4 N. Klopčič, I. Grimmer, F. Winkler, M. Sartory and A. Trattner, A review on metal hydride materials for hydrogen storage, *J. Energy Storage*, 2023, **72**, 108456.
5 T. Sato, H. Saitoh, R. Utsumi, J. Ito, Y. Nakahira, K. Obana, S. Takagi and S. Orimo, Hydrogen Absorption Reactions of Hydrogen Storage Alloy $LaNi_5$ under High Pressure, *Molecules*, 2023, **28**(3), 1256.
6 S. Y. Lee, J. H. Lee, Y. H. Kim, J. W. Kim, K. J. Lee and S. J. Park, Recent Progress Using Solid-State Materials for Hydrogen Storage: A Short Review, *Processes*, 2022, **10**(2), 304.
7 D. R. MacFarlane, P. V. Cherepanov, J. Choi, B. H. R. Suryanto, R. Y. Hodgetts, J. M. Bakker, *et al.*, A Roadmap to the Ammonia Economy, *Joule*, 2020, **4**(6), 1186–1205.
8 T. A. Abtew, B. C. Shih, P. Dev, V. H. Crespi and P. Zhang, Prediction of a multicenter-bonded solid boron hydride for hydrogen storage, *Phys. Rev. B*, 2011, **83**(9), 094108.
9 Y. Jiao, F. Ma, J. Bell, A. Bilic and A. Du, Two-Dimensional Boron Hydride Sheets: High Stability, Massless Dirac Fermions, and Excellent Mechanical Properties, *Angew. Chem., Int. Ed.*, 2016, **55**(35), 10292–10295.
10 B. Mortazavi, M. Makaremi, M. Shahrokhi, M. Raeisi, C. V. Singh, T. Rabczuk, *et al.*, Borophene hydride: a stiff 2D material with high thermal conductivity and attractive optical and electronic properties, *Nanoscale*, 2018, **10**(8), 3759–3768.
11 L. C. Xu, A. Du and L. Kou, Hydrogenated borophene as a stable two-dimensional Dirac material with an ultrahigh Fermi velocity, *Phys. Chem. Chem. Phys.*, 2016, **18**(39), 27284–27289.
12 H. Nishino, T. Fujita, N. T. Cuong, S. Tominaka, M. Miyauchi, S. Iimura, A. Hirata, N. Umezawa, S. Okada, E. Nishibori, A. Fujino, T. Fujimori, S. Ito, J. Nakamura, H. Hosono, T. Kondo, *et al.*, Formation and characterization of hydrogen boride sheets derived from MgB_2 by cation exchange, *J. Am. Chem. Soc.*, 2017, **139**(39), 13761–13769.
13 A. Fujino, S. Ito, T. Goto, R. Ishibiki, J. N. Kondo, T. Fujitani, J. Nakamura, H. Hosono and T. Kondo, Hydrogenated Borophene Shows Catalytic Activity as Solid Acid, *ACS Omega*, 2019, **4**(9), 14100–14104.
14 A. Fujino, S. Ito, T. Goto, R. Ishibiki, R. Osuga, J. N. Kondo, T. Fujitani, J. Nakamura, H. Hosono and T. Kondo, Ethanol–ethylene conversion mechanism on hydrogen boride sheets probed by *in situ* infrared absorption spectroscopy, *Phys. Chem. Chem. Phys.*, 2021, **23**(13), 7724–7734.
15 S. Gao, Y. Zhang, J. Bi, B. Wang, C. Li, J. Liu, *et al.*, 2D hydrogenated boride as a reductant and stabilizer for *in situ* synthesis of ultrafine and surfactant-free carbon supported noble metal electrocatalysts with enhanced activity and stability, *J. Mater. Chem. A*, 2020, **8**(36), 18856–18862.
16 S. Gao, H. Zhao, P. Gao, J. Bi, D. Liu, D. Zhu, *et al.*, Hydrogenated Boride-Assisted Gram-Scale Production of Platinum–Palladium Alloy Nanoparticles on Carbon Black for PEMFC Cathodes: A Study from a Practical Standpoint, *ACS Appl. Mater. Interfaces*, 2022, **14**(30), 34750–34760.
17 A. Saad, D. Liu, Y. Wu, Z. Song, Y. Li, T. Najam, *et al.*, Ag nanoparticles modified crumpled borophene supported Co_3O_4 catalyst showing superior oxygen evolution reaction (OER) performance, *Appl. Catal., B*, 2021, **298**, 120529.
18 X. Zeng, Y. Jing, S. Gao, W. Zhang, Y. Zhang, H. Liu, *et al.*, Hydrogenated borophene enabled synthesis of multielement intermetallic catalysts, *Nat. Commun.*, 2023, **14**(1), 7414.
19 S. Ito, T. Hirabayashi, R. Ishibiki, R. Kawamura, T. Goto, T. Fujita, *et al.*, Hydrogen Boride Sheets as Reductants and the Formation of Nanocomposites with Metal Nanoparticles, *Chem. Lett.*, 2020, **49**(7), 789–793.
20 N. Noguchi, S. Ito, M. Hikichi, Y. Cho, K. Goto, A. Kubo, *et al.*, Highly Dispersed Ni Nanoclusters Spontaneously Formed on Hydrogen Boride Sheets, *Molecules*, 2022, **27**(23), 8261.
21 R. Kawamura, R. Kawamura, A. Varadwaj, K. Kisu, R. Tanaka, A. Yamamoto, R. Ishibiki, S. Ito, T. Fujita, T. Tokunaga, O. Oki, Y. Fujimoto, M. Toyoda, S. Saito, T. Sato, S. Orimo, H. Hosono, I. Matsuda, M. Kotsugi, M. Miyauchi and T. Kondo, Enhanced Hydrogen Release from Hydrogen Boride Nanosheets *via* Carbon Doping, *Small Struct.*, 2025, **6**, e202500578.

22 R. Kawamura, N. T. Cuong, T. Fujita, R. Ishibiki, T. Hirabayashi, A. Yamaguchi, I. Matsuda, S. Okada, T. Kondo and M. Miyauchi, Photoinduced hydrogen release from hydrogen boride sheets, *Nat. Commun.*, 2019, **10**(1), 4880.
23 J. Takeshita, H. Tsurugi, A. Mauliana, A. Yamaguchi, T. Kondo and M. Miyauchi, Visible-Light-Induced Hydrogen Generation from Mixtures of Hydrogen Boride Nanosheets and Phenanthroline Molecules, *Adv. Sci.*, 2024, **11**(42), 2405981, DOI: 10.1002/advs.202405981.
24 C. Shimada, A. Yamaguchi, A. Mauliana, Y. Yang, H. Tsurugi, T. Kondo and M. Miyauchi, Visible-Light-Driven Hydrogen Release from Dye-Sensitized Hydrogen Boride Nanosheets, *ACS Appl. Mater. Interfaces*, 2024, **16**(27), 35225–35231.
25 A. Mauliana, A. Yamaguchi, T. Kondo and M. Miyauchi, Hydrogen Boride Sheets and Copper Nanoparticle Composites as a Visible-Light-Sensitive Hydrogen Release System, *Small*, 2024, **20**(49), 2404986.
26 S. Kawamura, A. Yamaguchi, K. Miyazaki, S. Ito, N. Watanabe, I. Hamada, T. Kondo and M. Miyauchi, Electrolytic Hydrogen Release from Hydrogen Boride Sheets, *Small*, 2024, **20**(27), 2310239.
27 M. Hikichi, J. Takeshita, J. Han, S. Ito, O. Oki, R. Tsuji, A. Hasegawa, S. Jeong, Y. Ito, I. Matsuda, H. Tsurugi, M. Miyauchi and T. Kondo, Enhanced Thermal- and Photostability of Trace Pyrazine-Incorporated Hydrogen Boride Nanosheets, *Small*, 2025, **21**, e06230.
28 N. J. Dudney and J. Li, Using all energy in a battery, *Science*, 2015, **347**(6218), 131–132.
29 H. Chen, M. Ling, L. Hencz, H. Y. Ling, G. Li and Z. Lin, Exploring Chemical, Mechanical, and Electrical Functionalities of Binders for Advanced Energy-Storage Devices, *Chem. Rev.*, 2018, **118**(18), 8936–8982.
30 A. Cholewinski, P. Si, M. Uceda, M. Pope and B. Zhao, Polymer Binders: Characterization and Development toward Aqueous Electrode Fabrication for Sustainability, *Polymers*, 2021, **13**(4), 631.
31 M. Yang, K. Cao, L. Sui, Y. Qi, J. Zhu and A. Waas, Dispersions of Aramid Nanofibers: A New Nanoscale Building Block, *ACS Nano*, 2011, **5**(9), 6945–6954, DOI: 10.1021/nn2014003.
32 S. Zafar, S. Furuhata, Y. Ugata, T. Komagata and N. Yabuuchi, Meta-aramid resin as functional binder and its applications for bipolar-type aqueous batteries, *Mater. Today Energy*, 2025, **52**, 101962, DOI: 10.1016/j.mtener.2025.101962.
33 P. Flouda, S. Oka, D. Loufakis, D. C. Lagoudas and J. L. Lutkenhaus, Structural Lithium-Ion Battery Cathodes and Anodes Based on Branched Aramid Nanofibers, *ACS Appl. Mater. Interfaces*, 2021, **13**, 34807–34817, DOI: 10.1021/acsami.1c06413.
34 S. R. Kwon, J. Harris, T. Zhou, D. Loufakis, J. G. Boyd and J. L. Lutkenhaus, Mechanically Strong Graphene/Aramid Nanofiber Composite Electrodes for Structural Energy and Power, *ACS Nano.*, 2017, **11**(7), 6682–6690.
35 K. I. M. Rojas, N. T. Cuong, H. Nishino, R. Ishibiki, S. Ito, M. Miyauchi, Y. Fujimoto, S. Tominaka, S. Okada, H. Hosono, B. A. Nelson, T. Kondo, Y. Morikawa and I. Hamada, Chemical stability of hydrogen boride nanosheets in water, *Commun. Mater.*, 2021, **2**(1), 81.
36 S. Ito, M. Hikichi, N. Noguchi, M. Yuan, Z. Kang, K. Fukuda, I. Matsuda, M. Miyauchi and T. Kondo, Effective treatment of hydrogen boride sheets for long-term stabilization, *Phys. Chem. Chem. Phys.*, 2023, **25**(22), 15531–15538.
37 S. Tominaka, R. Ishibiki, A. Fujino, K. Kawakami, K. Ohara, T. Masuda, *et al.*, Geometrical Frustration of B-H Bonds in Layered Hydrogen Borides Accessible by Soft Chemistry, *Chem*, 2020, **6**(2), 406–418.
38 A. Bashir, M. Maqbool, R. Lv, A. Usman, W. Aftab, H. Niu, L. Kang and S. Bai, Engineering of Interfacial Interactions Among BN And CNT Hybrid Towards Higher Heat Conduction Within TPU Composites, *Composites, Part A*, 2023, **167**, 107428.
39 T. Nagai, A. Mauliana, K. Kobayashi, A. Yamaguchi, K. Miyazaki, Y. Yang, *et al.*, Broad-spectrum antimicrobial effects of hydrogen boride nanosheets, *J. Mater. Chem. B*, 2025, **13**(19), 5723–5733.
40 J. Fan, Z. Shi, L. Zhang, J. Wang and J. Yin, Aramid nanofiber-functionalized graphene nanosheets for polymer reinforcement, *Nanoscale*, 2012, **4**(22), 7046.